Available online at www.sciencedirect.com
SCIENCE DIRECT®
Journal of Sound and Vibration 269 (2004) 295–325
JOURNAL OF SOUND AND VIBRATION
www.elsevier.com/locate/jsvi

Development of elastic force model for wheel/rail contact problems

Ahmed A. Shabana[a,*], Khaled E. Zaazaa[a], José L. Escalona[b], Jalil R. Sany[c]

[a] *Department of Mechanical Engineering MC 251, University of Illinois at Chicago, 2039 Engineering Research Facility, 842 West Taylor Street, Chicago, IL 60607-7022, USA*

[b] *Department of Mechanical and Materials Engineering, University of Seville, Camino de los Descubrimientos s/n, 41092, Seville, Spain*

[c] *Center for Automated Mechanics (CAM), 5242 West Cenmark Rd., Cicero, IL 60804, USA*

Received 13 June 2002; accepted 16 December 2002

Abstract

In this investigation, a new formulation for the wheel/rail contact problem based on the elastic force approach is presented. Crucial to the success of any elastic force formulation for the wheel/rail contact problem is the accurate prediction of the location of the contact points. To this end, features of multibody formulations that allow introducing additional differential equations are exploited in this investigation in order to obtain a good estimate of the rail arc length travelled by the wheel set. In the formulation presented in this paper, four parameters are used to describe the wheel and the rail surfaces. In order to determine the location of the points of contact between the wheel and the rail, a first order differential equation for the rail arc length is introduced and is integrated simultaneously with the multibody equations of motion of the wheel/rail system. The method presented in this paper allows for multiple points of contact between the wheel and the rail by using an optimized search for all possible contact points. The normal contact forces are calculated and used with non-linear expressions for the creepages to determine the creep forces. The paper also discusses two different procedures for the analysis of the two-point contact in the wheel/rail interaction. Numerical results obtained using the elastic force model are presented and compared with the results obtained using the constraint approach.

1. Introduction

Two approaches are commonly used for solving the problem of wheel/rail contact in railroad dynamics [1–6]. The first is the *elastic approach* in which the wheel is assumed to have six degrees

*Corresponding author. Tel.: +312-996-3600; fax: +312-413-0447.
E-mail address: shabana@uic.edu (A.A. Shabana).

0022-460X/03/$ - see front matter © 2003 Elsevier Ltd. All rights reserved.
doi:10.1016/S0022-460X(03)00074-9

of freedom with respect to the rail. The normal contact forces are defined using Hertz's contact theory or in terms of assumed stiffness and damping coefficients [9,10]. The second approach is the *constraint approach* in which non-linear kinematic contact constraint equations are introduced, leading to a model in which the wheel has five degrees of freedom with respect to the rail [7,8].

Since in the elastic approach the wheel is assumed to have six degrees of freedom with respect to the rail, separation between the wheel and the rail is allowed. However, one of the main problems encountered when using the elastic approach is the difficulty in determining the location of the contact point on line. In most elastic force models, the three-dimensional contact problem is reduced, for the sake of efficiency, to a two-dimensional problem when the location of the contact points is searched for. In the case of a wheel set travelling on a curved track with specified or non-specified velocity, accurate prediction of the rail arc length travelled by the wheel can be crucial in determining the correct location of the point of contact on the wheel and the rail. It is the objective of this paper to address this important problem, and propose a computer methodology that allows for accurate prediction of the co-ordinates of the contact points when the elastic approach is used in the analysis of the wheel/rail contact.

In this paper, a new formulation based on the elastic force model is developed for the wheel/rail contact problem. In this formulation, four surface parameters are used to describe the geometry of the wheel and rail surfaces. The equations of motion are formulated using the Lagrangian approach [11]. In order to be able to accurately determine the location of the contact points on the wheel and the rail, a first order differential equation expressed in terms of the rail arc length and the wheel generalized co-ordinates and velocities is introduced. The solution of this system of differential equations defines the system-generalized co-ordinates and velocities as well as the arc length travelled by the wheel. Knowing this arc length, the three-dimensional kinematic problem can be simplified to determine the location of the contact point on the wheel and the rail. The method can be used in the case of straight and curved tracks and allows for general spline function representation of the wheel and rail surface profiles. The co-ordinates and velocities of the contact points are also used to determine the non-linear expressions of the creepages. Using the non-linear creepage expressions and the normal forces, the tangential creep forces are calculated and used to define the generalized creep forces associated with the system generalized co-ordinates. Numerical results obtained using the proposed elastic force approach are presented and compared with the results obtained using the contact constraint approach [7,8].

This paper is organized as follows: in Section 2, the fundamental differences between the constraint method and the elastic force method are explained. Section 3 is devoted to the kinematic representation of the wheel and rail profiles used in both methods. Section 4 describes the algorithms used to determine the contact points, and Section 5 summarizes the procedure used in this paper to calculate the contact forces in the elastic force method. In Section 6, the form of the dynamic equations used in the elastic force method is presented, while a brief review of the contact constraint formulation is presented in Section 7. Section 8 explains two different methods used for the analysis of the two-point contact in wheel/rail interaction; the *elastic method* and the *hybrid method*. Numerical results of a single wheel set travelling on tangent and curved tracks are presented in Section 9. Summary and conclusions of this work are provided in Section 10.

2. Contact constraint and elastic approaches

In rigid-body mechanics, two different approaches can be used to describe the contact between bodies: the constraint method and the elastic method. For bodies with non-conforming and smooth geometries, it is assumed in both approaches that contact occurs at a single material point on each body. The contact forces are assumed to be concentrated, and applied at these contact points. Apart from the numerical treatment of the contact problem, that will be discussed in more details in later sections of this paper, these two approaches differ in three physical aspects: the determination of the contact point, the evaluation of the normal contact forces and the indentation allowed between the bodies in contact. These differences are illustrated in Fig. 1 and explained below.

2.1. Contact location

In the constraint method, the contact points on both solids coincide as guaranteed by imposing the kinematic contact constraints. In the elastic method, the contact points do not, in general, coincide. The contact point on one body has to be located inside the volume of the other body since penetration occurs. In this case, the contact points can be selected from those points belonging to the volume that the two solids share as the points of maximum indentation (maximum normal distance).

2.2. Determination of normal contact forces

In the constraint method, normal contact forces are obtained as the reaction forces (Lagrange multipliers) resulting from imposing the contact constraint equations. This means that the contact forces are those forces that are necessary to guarantee the dynamic equilibrium and satisfy the constraints imposed on the motion of the system. In the elastic method, normal contact forces are evaluated as functions of the indentation. Contact forces are treated as visco-elastic forces that can be expressed as functions of the co-ordinates and velocities of the two bodies.

2.3. Penetration between bodies

In the constraint method, no penetration is allowed between the bodies since it is assumed that the surfaces do no experience any deformation. In the elastic method, on the other hand,

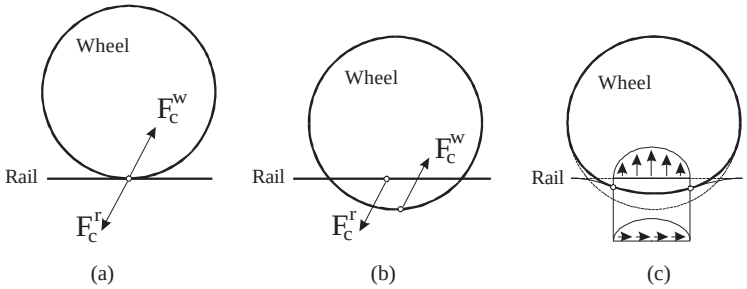

Fig. 1. Methods for rigid body contact: (a) constraint method, (b) elastic method, (c) real configuration.

penetration is assumed to occur and is used to determine the contact forces. The contact forces are equal to zero if there is no penetration. The penetration that occurs can be used as the basis to develop, in the elastic method, a simple procedure to evaluate the local deformation of the bodies in contact. Although bodies are assumed to be rigid, the contact forces calculated in the elastic method are those forces that would occur if the penetration were due to a local elastic deformation, and the calculated contact forces are usually equivalent to those forces that would appear if the bodies in contact would be pressed against each other by external static forces.

3. Track and wheel geometries

In the general formulation of the contact between a rigid wheel and a rigid rail, two surface parameters are used to describe the geometry of each of the two surfaces in contact. The two surface parameters s_1^r and s_2^r are used to describe the geometry of the rail surface, and s_1^w and s_2^w are the two surface parameters used to describe the wheel surface, as shown in Fig. 2. The position vector of a point on the wheel or the rail can be defined in the respective body co-ordinate system as

$$\bar{\mathbf{u}}^l = \bar{\mathbf{u}}^l(s_1^l, s_2^l), \tag{1}$$

where $l = w$ or r, and superscript w and r refer to wheel and rail, respectively.

3.1. Track geometry

Fig. 3 shows a curved rail r with an arbitrary geometry and surface profile. The surface geometry of the rail r can be described in the most general case using the two surface parameters s_1^r and s_2^r, where s_1^r represents the rail arc length and s_2^r is the surface parameter that defines the rail profile, as shown in Fig. 2. For convenience and simplicity, the surface parameter s_2^r is defined in a profile co-ordinate system $X^{rp}Y^{rp}Z^{rp}$, also shown in Figs. 2 and 3. The location of the origin and

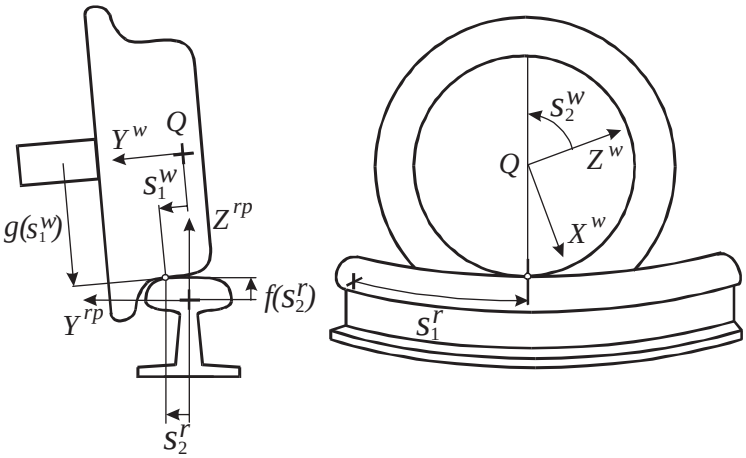

Fig. 2. Surface parameters.

the orientation of the profile co-ordinate system, defined, respectively, by the vector $\mathbf{R}^{rp}$ and the transformation matrix $\mathbf{A}^{rp}$, can be uniquely determined using the surface parameter s_1^r [12]. Using this description, the global position vector of an arbitrary point on the surface of the rail r can be written as [12]

$$\mathbf{r}^r = \mathbf{R}^r + \mathbf{A}^r(\mathbf{R}^{rp} + \mathbf{A}^{rp}\bar{\mathbf{u}}^{rp}), \tag{2}$$

where $\mathbf{R}^r$ is the global position vector of the origin of the rail co-ordinate system $X^rY^rZ^r$, $\mathbf{A}^r$ is the transformation matrix that defines the orientation of the rail co-ordinate system, and $\bar{\mathbf{u}}^{rp}$ is the local position vector that defines the location of the arbitrary point on the rail surface with respect to the profile co-ordinate system. Note that due to the above-mentioned description of the rigid rail geometry, one has

$$\mathbf{R}^{rp} = \mathbf{R}^{rp}(s_1^r), \quad \mathbf{A}^{rp} = \mathbf{A}^{rp}(s_1^r), \quad \bar{\mathbf{u}}^{rp} = [\,0 \quad s_2^r \quad f(s_2^r)\,]^{\mathrm{T}}, \tag{3}$$

where f is the function that defines the rail profile. The transformation matrix $\mathbf{A}^{rp}$ can be expressed in terms of three Eulerian angles, each of which can be expressed uniquely in terms of the surface parameter s_1^r. Note also that the rail geometry described by the preceding two equations allows for a general displacement of the rail with respect to the global co-ordinate system. The method developed in this investigation allows for an arbitrary spline representation for the rail and accounts for the rail cant, elevation, and gage variation.

3.2. Wheel geometry

Fig. 4 shows a wheel with an arbitrary surface profile. The surface geometry of the wheel w can be described using the two surface parameters s_1^w and s_2^w. The surface parameters are defined in a wheel set co-ordinate system $X^wY^wZ^w$, also shown in the figure. The surface parameter s_1^w defines

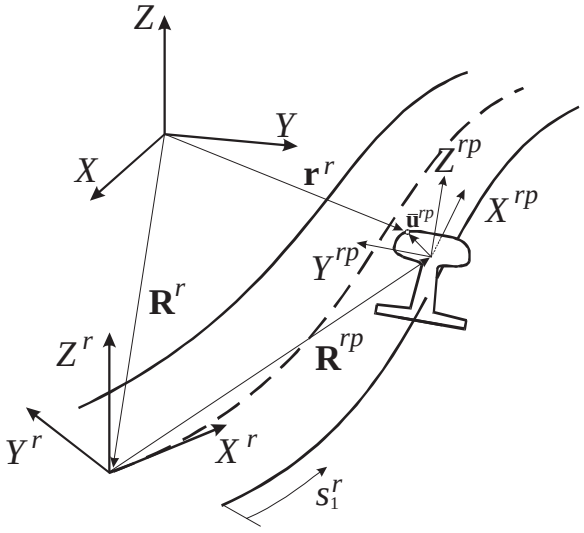

Fig. 3. Track geometry.

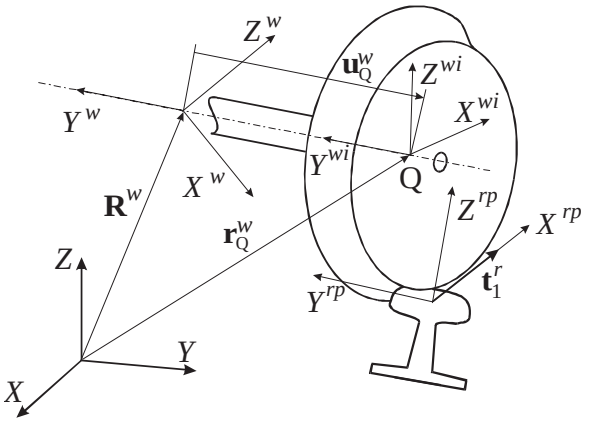

Fig. 4. Wheel geometry.

the wheel profile and s_2^w represents the rotation of the contact point, as shown in Fig. 2. The location of the origin and the orientation of the wheel set co-ordinate system are defined respectively by the vector $\mathbf{R}^w$ and the transformation matrix $\mathbf{A}^w$. Using this description, the global position vector of an arbitrary point on the surface of the wheel w can be written as

$$\mathbf{r}^w = \mathbf{R}^w + \mathbf{A}^w \bar{\mathbf{u}}^w, \tag{4}$$

where $\bar{\mathbf{u}}^w$ is the local position vector that defines the location of the arbitrary point on the wheel surface with respect to the wheel set co-ordinate system. In the case of the right wheel, this vector is defined as

$$\bar{\mathbf{u}}^w = [\, g(s_1^w) \sin s_2^w \quad -L + s_1^w \quad g(s_1^w) \cos s_2^w \,]^{\mathrm{T}}, \tag{5}$$

where g is the function that defines the wheel profile, and L is the distance between the origin of the wheel set co-ordinate system and point Q of the wheel, as shown in Figs. 2 and 4.

4. Determination of the contact points

As previously pointed out, one of the important problems encountered in the use of the elastic force model is the accurate determination of the point on the wheel surface that comes into contact with the rail. Crucial in the development of a successful computational strategy is accurate prediction of the wheel and rail surface parameters that determine the points of contact. The method described in this section allows for identifying an arbitrary number of contact points between surfaces that have arbitrary geometry. In the search method used in this investigation, the contact surface geometry are defined in wheel and rail *surface profile co-ordinate systems*, as shown in Fig. 2, using discrete nodal points and a spline function representation. A preprocessor is used to define the location of these nodal points with respect to the body (wheel or rail) co-ordinate system assuming that the orientation of the surface profile co-ordinate system remains constant with respect to the body co-ordinate system.

The search for the contact points consists of the following three steps:

1. Calculation of the rail arc length s_1^r travelled by the wheel. The parameter s_1^r defines the rail cross section in which the points of contact are located.
2. Calculation of the wheel angular parameter s_2^w. The parameter s_2^w defines the wheel diametric section in which the points of contact are located.
3. Search for the contact points. In this phase the rail parameter s_2^r and the wheel parameter s_1^w of the points of contact are determined. This phase of the search starts once the sections of the wheel and rail in which the contact points are located are determined. The exact position of the contact points is determined in this phase of the search.

The algorithms used for the three steps of the search are described in the following subsections.

4.1. Calculation of the rail arc length travelled by the wheel

In the search algorithm used in this investigation to determine the contact points, a selected point Q on the center of the wheel is used first to determine the rail space curve parameter s_1^r. It is assumed that the rate of change of the rail parameter s_1^r is equal to the projection of the velocity of this point on the tangent along the longitudinal rail direction. The position of this selected point with respect to the wheel co-ordinate system is defined as

$$\mathbf{u}_Q^w = \mathbf{r}_Q^w - \mathbf{R}^w, \tag{6}$$

where $\mathbf{r}_Q^w$ is the global position vector of point Q, and $\mathbf{R}^w$ is the global position of the origin of the wheel co-ordinate system. The global velocity of this point on the wheel is defined as

$$\dot{\mathbf{r}}_Q^w = \dot{\mathbf{R}}^w + \boldsymbol{\omega}^w \times \mathbf{u}_Q^w, \tag{7}$$

where $\boldsymbol{\omega}^w$ is the angular velocity vector of the wheel defined in the global co-ordinate system. Knowing the tangent $\mathbf{t}_1^r$ to the space curve of the rail at the current s_1^r, the following first order differential equation can be defined:

$$\dot{s}_1^r = \dot{\mathbf{r}}_Q^{w\mathrm{T}} \mathbf{t}_1^r. \tag{8}$$

This differential equation is solved simultaneously with the differential and algebraic equations of the multibody system in order to determine s_1^r that is used for the search for the point of contact between the wheel and the rail. Clearly, one needs to introduce a number of arc length first order differential equations (Eq. (8)) equal to the number of wheels in the dynamic model.

Knowing the current arc length s_1^r, the location and orientation of the rail surface profile co-ordinate system that corresponds to a possible contact with the wheel can be defined in the rail co-ordinate system. As previously discussed, let $\mathbf{R}^{rp}$ and $\mathbf{A}^{rp}$ define, respectively, the location of the origin and orientation of the rail surface profile co-ordinate system, and let $\bar{\mathbf{u}}^{rp}$define the position vector of an arbitrary point on the surface profile with respect to the surface profile co-ordinate system. The global position vector of this arbitrary point can be defined using Eq. (2).

4.2. Calculation of the wheel angular parameter

For the calculation of the wheel parameter s_2^w of the contact points, an intermediate co-ordinate system $X^{wi}Y^{wi}Z^{wi}$ which does not rotate with the wheel, and it has the same wheel roll and yaw rotations is determined. Fig. 4 shows this co-ordinate system as well as the wheel body fixed co-ordinate system $X^wY^wZ^w$ and the rail profile co-ordinate system $X^{rp}Y^{rp}Z^{rp}$, previously introduced. The co-ordinate system $X^{wi}Y^{wi}Z^{wi}$ is determined as follows. The axis Y^{wi} is selected to be the same as the current wheel Y^w-axis, thereby ensuring that the two co-ordinate systems have the same roll and yaw angles. Note that the axis Y^w is known as the result of the dynamic simulation that defines the wheel orientation. The axis X^{wi} is defined by the unit vector $\mathbf{i}^{wi}$, where

$$\mathbf{i}^{wi} = \mathbf{j}^{wi} \times \mathbf{k}^{rp}, \tag{9}$$

and where $\mathbf{j}^{wi}$ is a unit vector along the Y^{wi}-axis, and $\mathbf{k}^{rp}$ is a unit vector along the Z^{rp}-axis of the rail profile co-ordinate system previously described. Using the preceding equation, the Z^{wi}-axis can be defined using the unit vector $\mathbf{k}^{wi}$ defined as

$$\mathbf{k}^{wi} = \mathbf{i}^{wi} \times \mathbf{j}^{wi}. \tag{10}$$

This completes the definition of the orthogonal triad $X^{wi}Y^{wi}Z^{wi}$. The point of contact on the wheel is assumed to be located at the plane formed by the Y^{wi}- and Z^{wi}-axes. This plane determines the diametric cross-section of the wheel in which the contact point is assumed to be located. Therefore, the parameter s_2^w is obtained as the angle between the wheel set fixed axis Z^w and the intermediate axis Z^{wi}.

4.3. Search for the contact points

In order to determine the points of contact between the wheel and the rail, the global position vectors of the nodal points that define the wheel and rail profiles are determined as described in the previous subsections. The distance between the points on the wheel and the points on the rail are calculated and used with a user specified tolerance criterion to determine the points of contact. Since this search can lead to a very large number of contact points, an optimized procedure that improves the computational efficiency must be adopted. In this investigation, the contact points are grouped in batches. A batch is a collection of sets of pairs of nodal points on the wheel and rail that have non-zero penetration. While the algorithm developed in this study allows for an arbitrary number of contact batches, a limit of two contact batches as shown in Fig. 5 is assumed in the numerical investigation presented in this paper. The two points (one on the wheel and one on the rail) that lead to the maximum indentation are selected as the points of contact for any given batch. The number of points of contact between the wheel and the rail is assumed to be equal to the number of the contact batches. That is, the algorithm used in this investigation to search for the contact points allows, in general, for multiple contacts between the wheel and the rail.

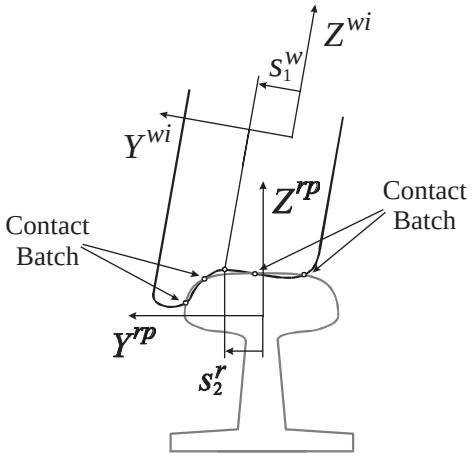

Fig. 5. Profile co-ordinate systems for wheel and rail.

5. Calculation of contact forces

In this investigation, it is assumed that each contact area has an elliptic shape. The surface parameters are used to determine the principal curvatures at the point of contact. The normal contact forces and the dimension of the contact ellipses are determined using Hertz's contact theory [13]. By providing the penetration at the contact point as well as the material properties of the wheel and the rail, the normal contact forces can be calculated. The direction of the normal force is determined as the direction of the normal to the surface at the contact point. The dimensions of the contact ellipses and the normal forces are required in order to calculate the creep forces that are determined using Kalker's USETAB routine. No linearization is used in the calculations of the creepages used to determine the creep forces. The generalized normal and creep forces associated with the system generalized co-ordinates are determined and introduced to the multibody system dynamic equations of motion as described in the following section.

In the evaluation of the normal contact force, in addition to the Hertzian component, which is a function of the indentation, a damping force proportional to the velocity of indentation is included. The expression of the normal force used in this investigation is given by

$$F = F_h + F_d = -K_h\delta^{3/2} - C\dot{\delta}|\delta|, \tag{11}$$

where δ is the indentation, F_h is the Herzian (elastic) contact force, F_d is the damping force, K_h is the Hertzian constant that depends on the surface curvatures and the elastic properties, and C is a damping constant. The velocity of indentation $\dot{\delta}$ is evaluated as the dot product of the relative velocity vector of the contact points on the wheel and rail and the normal vector to the surface at the contact point. The expression of the damping component of the contact force is obtained by modifying the damping force proposed by Lee and Wang [14]. The reason for including the factor $|\delta|$ is to guarantee that the contact force is zero when the indentation is zero. The damping coefficient C has to be selected in such a way that no tensile forces are generated when the indentation decreases (restitution phase).

6. Formulation of the dynamic equations

For a railroad vehicle model, the augmented form of the equations of motion can be written as [11]

$$\begin{bmatrix} \mathbf{M} & \mathbf{C}_{\mathbf{q}}^{\mathrm{T}} \\ \mathbf{C}_{\mathbf{q}} & \mathbf{0} \end{bmatrix} \begin{bmatrix} \ddot{\mathbf{q}} \\ \lambda \end{bmatrix} = \begin{bmatrix} \mathbf{Q} \\ \mathbf{Q}_d \end{bmatrix}, \tag{12}$$

where $\mathbf{M}$ is the system mass matrix, $\mathbf{C}_{\mathbf{q}}$ is the Jacobian matrix of the kinematic constraints, $\mathbf{q}$ is the vector of the system generalized co-ordinates, λ is the vector of Lagrange multipliers, $\mathbf{Q}$ is a vector that includes external, applied contact, creep, and centrifugal and Coriolis forces, and $\mathbf{Q}_d$ is the vector that results from the differentiation of the constraint equations twice with respect to time, that is

$$\mathbf{C}_{\mathbf{q}}\ddot{\mathbf{q}} = \mathbf{Q}_d. \tag{13}$$

The vector of the kinematic constraint equations $\mathbf{C}(\mathbf{q}, t) = \mathbf{0}$ describes mechanical joints as well as specified motion trajectories that include driving constraints. Such driving constraints include the specified forward velocity of the wheel sets.

As previously pointed out, crucial to the success of the elastic force model developed in this investigation for the dynamic simulation of the interaction between the wheel and the rail is the accurate prediction of the rail arc length travelled by the wheel. The new method proposed in this investigation allows for such an accurate prediction by introducing an arc length first order differential equation that depends non-linearly on the wheel generalized co-ordinates and the rail geometry. This first order differential equation, which is defined by Eq. (8), is integrated simultaneously with the state equations obtained for the wheel/rail system using Eq. (12). The numerical integration of this new combined system of equations defines the system generalized co-ordinates and velocities as well as the rail arc length s_1^r travelled by the wheel. This parameter s_1^r is used as the basis for the search for the contact points as previously described in this paper.

7. Constraint formulation

In later sections of this paper, numerical results are presented in order to compare between the elastic contact force model presented in this paper and the constraint force model presented in previous publications [7,8]. These two conceptually different approaches lead to different formulations that require different numerical solution procedures. In this section, the constraint contact formulation is briefly reviewed in order to shed light on the basic differences between the two approaches. To this end, the geometric description of the wheel and rail surfaces is assumed to be the same as the one used in the elastic method described in this paper.

Five kinematic constraint equations are used to describe the general contact between two rigid bodies [7,8]. Three of these five constraints, called *contact point constraints*, impose the conditions that two points on the two bodies coincide during the dynamic motion as shown in Fig. 6 while avoiding penetration and separation, that is

$$\mathbf{r}^w = \mathbf{r}^r. \tag{14}$$

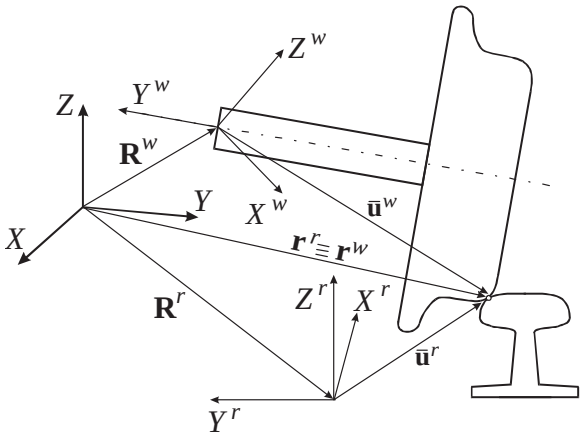

Fig. 6. Position of contact point.

The remaining two constraints, called *orientation constraints*, impose the condition that the normals to the surfaces at the contact point are parallel, that is

$$\mathbf{n}^w = \alpha \mathbf{n}^r, \tag{15}$$

where $\mathbf{n}^w$ and $\mathbf{n}^r$ are, respectively, the normals to the wheel and the rail surfaces at the contact point, and α is a scalar. Since four new surface parameters are introduced, the preceding independent five contact constraint equations can be used to eliminate only one generalized degree of freedom. Therefore, in this formulation, the wheel has five degrees of freedom with respect to the rail.

In general, the kinematic constraint equations, including the contact constraints, imposed on the motion of a multibody system can be expressed in the following vector form:

$$\mathbf{C}(\mathbf{q}, \mathbf{s}, t) = \mathbf{0}, \tag{16}$$

where $\mathbf{C}$ is the vector of constraint functions, $\mathbf{q}$ is the vector of the system generalized coordinates, $\mathbf{s}$ is the vector of the system non-generalized surface parameters, and t is time. Differentiating the preceding equation twice with respect to time and combining the resulting acceleration equations with the Lagrangian form of the equations of motion expressed in terms of Lagrange multipliers, one obtains the following augmented form of the equations of motion of the multibody system subject to contact constraints [7,8]:

$$\begin{bmatrix} \mathbf{M} & \mathbf{0} & \mathbf{C}_\mathbf{q}^\mathrm{T} \\ \mathbf{0} & \mathbf{0} & \mathbf{C}_\mathbf{s}^\mathrm{T} \\ \mathbf{C}_\mathbf{q} & \mathbf{C}_\mathbf{s} & \mathbf{0} \end{bmatrix} \begin{bmatrix} \ddot{\mathbf{q}} \\ \ddot{\mathbf{s}} \\ \lambda \end{bmatrix} = \begin{bmatrix} \mathbf{Q} \\ \mathbf{0} \\ \mathbf{Q}_d \end{bmatrix}, \tag{17}$$

where $\mathbf{M}$ is the system mass matrix, λ is the vector of Lagrange multipliers, $\mathbf{Q}$ is a vector that includes external, creep, and centrifugal and Coriolis forces, and $\mathbf{Q}_d$ is a quadratic velocity vector that results from differentiating the kinematic constraints twice with respect to time [11]. Note

that the preceding augmented form of the equations of motion is expressed in terms of the generalized co-ordinates **q** as well as the non-generalized surface parameters **s** and their time derivatives.

In the general contact constraint formulation discussed in this section, the generalized co-ordinates and non-generalized surface parameters are solved simultaneously. That is, the effect of the changes of the surface parameters on the system-generalized co-ordinates is taken into consideration without assumptions or simplifications. Some other formulations ignore, for the sake of efficiency, the effect of the changes of all or some of the non-generalized surface parameters on the system-generalized co-ordinates. In these other formulations, at a given configuration of the wheel set, the geometric problem is solved by formulating a set of algebraic constraint equations that are used to determine the surface parameters for a given set of generalized co-ordinates of the wheel set. Using these surface parameters, the location of the contact point on the wheel and the rail can be determined. By using this approach the effect of the changes in the generalized co-ordinates on the non-generalized surface parameters is taken into consideration, while the effect of the changes of the surface parameters on the generalized co-ordinates is neglected. In such formulations that account for partial coupling between the generalized co-ordinates and non-generalized surface parameters, the order of the partial derivatives with respect to the surface parameter can be less than the third order required by the general contact formulation used in this investigation [7,8].

The main features of the contact constraint formulation used in this investigation can then be summarized as follows [7,8]:

1. The surface parameters are introduced in order to obtain a general formulation for the contact problem that allows predicting the location of the contact point on line. These surface parameters are treated as non-generalized co-ordinates since there is no inertia or forces associated with them.
2. The non-linear contact constraints are solved using an iterative Newton–Raphson algorithm in order to guarantee the existence of one contact between the wheel and the rail. Using the solution of the non-linear algebraic constraint equations, the contact constraint equations at the acceleration level are augmented to the system differential equations using the technique of Lagrange multipliers.
3. In the augmented formulation of the contact problem, Lagrange multipliers are used to determine the normal contact forces that enter into the calculations of the creep forces.
4. Higher order derivatives with respect to the surface parameters are required in order to impose the contact constraints at the acceleration level.
5. In the contact constraint formulation, it is assumed that there is no separation between the wheel and the rail. Normal contact forces obtained using Lagrange multipliers can be compressive or tensile forces. Tensile contact forces are not physically meaningful in wheel/rail problems but they can be used to predict wheel lift.

In the augmented formulations based on the *general constraint approach* that accounts for the complete dynamic coupling between the generalized and non-generalized co-ordinates, the degrees of freedom of the system are determined using a numerical procedure based on the numerical structure of the contact constraint Jacobian matrix. Several numerical studies have demonstrated

that the optimum set of the system degrees of freedom selected by the computer includes non-generalized surface parameters. Therefore, while the surface parameters have no inertia or forces associated with them, the optimum set of the independent state equations can include surface parameter state equations that are integrated simultaneously with other differential equations. The numerical integration determines the independent generalized co-ordinates and non-generalized surface parameters. Dependent co-ordinates and surface parameters are determined using the kinematic contact constraints.

8. Two-point contact problem

The simulation of the two-point contact between a wheel and a rail is one of the most difficult problems in the analysis of railroad vehicle systems. The two-point contact scenario that includes a flange contact is important in the analysis of curving behavior, hunting instability and derailment. The forces that result from the second point of contact influences the forces at the first point of contact, and these second point of contact forces can have a significant effect on the railroad vehicle dynamics and instability.

In this paper, two conceptually different methods are discussed for the analysis of the wheel/rail interaction. The first is the elastic force model that allows six degrees of freedom for the wheel with respect to the rail. This method also allows for the wheel lift. As described in this paper, a search is made in order to determine the contact batches and the contact points. Therefore, the elastic force model can be directly used to study the two-point contact by limiting the number of contact batches to two. The forces at the two contact points can be calculated as previously described in this paper.

A second method that can be used in the analysis of the two-point contact is a hybrid method. In this hybrid method, which allows only five degrees of freedom for the wheel with respect to the rail, the first point of contact is predicted using the contact constraint approach, while the second point of contact is determined using the elastic approach. The second point of contact is obtained by numerically searching for a point of contact different from the first point that is determined using the kinematic contact constraints. In the hybrid method, the normal force at the first point of contact is determined using Lagrange multipliers, while the normal force at the second point of contact is determined using the elastic approach described in this paper.

The second point of contact between the wheel and the rail can be located in a plane different from the plane that contains the centerline of the wheel and the first point of contact due to the yaw rotation of the wheel set. This contact configuration is known as the *lead* or *lag contact*. Considering this contact scenario is important in curve negotiation. Fig. 7 shows the location of the second point of contact at the right wheel in case of the lead contact. As can be observed, the diametric section that contains the second contact point on the wheel makes an angle Δs_2^w with the diametric section that contains the first contact point. Also, the section of the rail that contains the second point of contact is located at a distance Δs_1^r of the section that contains the first point of contact. Lag contact occurs when the values Δs_2^w and Δs_1^r are negative. In the method used in this investigation, the search process used is able to detect the lead and lag contacts and, therefore, the values Δs_2^w and Δs_1^r can be evaluated.

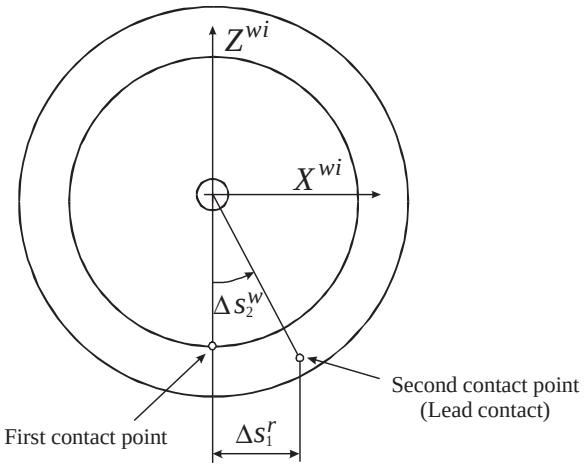

Fig. 7. Lead and lag contact.

9. Examples and numerical results

In this section, examples are presented in order to demonstrate the use of the formulations and numerical procedures discussed in this paper. These examples include the results of wheel set hunting at low and high speeds as well as the results of two-point contact analysis. Comparison between the results obtained using the elastic approach and the constraint approach is made.

9.1. Low-velocity hunting

A wheel set that travels on a tangent track with specified constant forward velocity is used as an example to study hunting at low speeds. The simulation results are obtained using two different methods: the elastic force model and the hybrid model. The wheel set mass is assumed to be 1568 kg, the moments of inertia are assumed to be $I_{yy} = 168\,\mathrm{kg\,m^2}$, $I_{xx} = I_{zz} = 656\,\mathrm{kg\,m^2}$. The wheels are assumed to be profiled with approximate conicity of 1/40, while the rail profile is assumed to be of the AREA type. The wheel and rail profiles are shown in Fig. 8. The coefficient of friction between the wheel and the rail is assumed to be 0.5. The wheel co-ordinate system and dimensions of the wheel and track are shown in Fig. 9. The constrained forward velocity of the wheel set is assumed to be $V = 10\,\mathrm{m/s}$. The wheel set is assumed to have an initial lateral velocity $v_y = -8\,\mathrm{mm/s}$. All other initial conditions are assumed to be zero. Note that in this example, because of the low speed, the wheel set does not experience a flange contact and the hybrid method simply reduces to the constraint method.

Fig. 10 shows the wheel set angular velocity as a function of time. The results presented in this figure are obtained using the constraint and elastic methods. These results show that the angular velocity changes linearly from zero to 21.88 rad/s in the time interval (0, 1.05 s). The angular velocity remains approximately constant afterwards. The results of a simple analytical analysis using Coulomb friction agree with the results presented in Fig. 10. Fig. 11 shows the forces and moments that act on the wheel set during the period in which sliding occurs. The free body diagram shown in this figure includes the inertia forces and the force F due to the driving

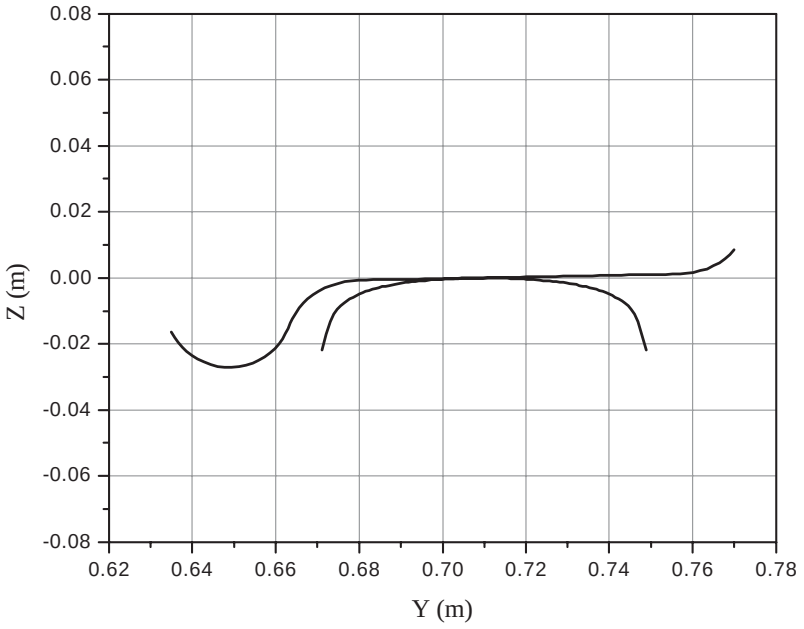

Fig. 8. Wheel and rail profiles.

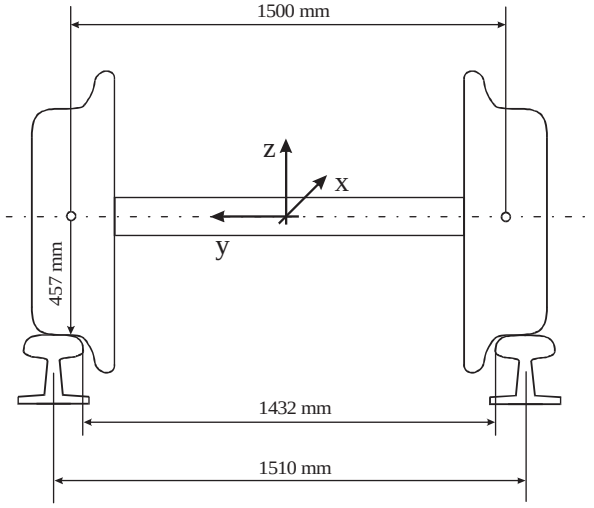

Fig. 9. Geometry of wheel set and rails.

constraint. The normal contact force N is equal to the weight of the wheel set, and the horizontal contact force is equal to μmg. Taking the moments about an axis passing through the center of the wheel set, the angular acceleration during the period of sliding can be obtained as follows:

$$\alpha = \frac{\mu mgR}{I}, \tag{18}$$

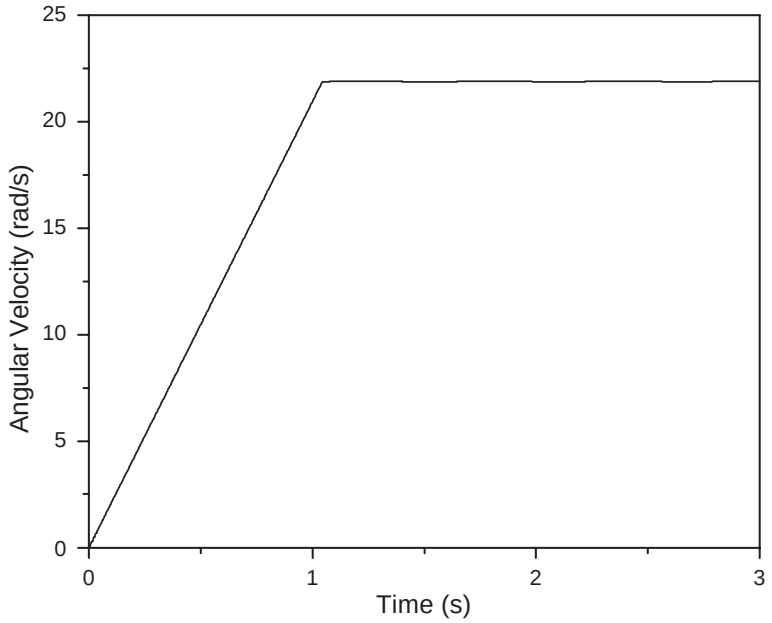

Fig. 10. Wheel set angular velocity.

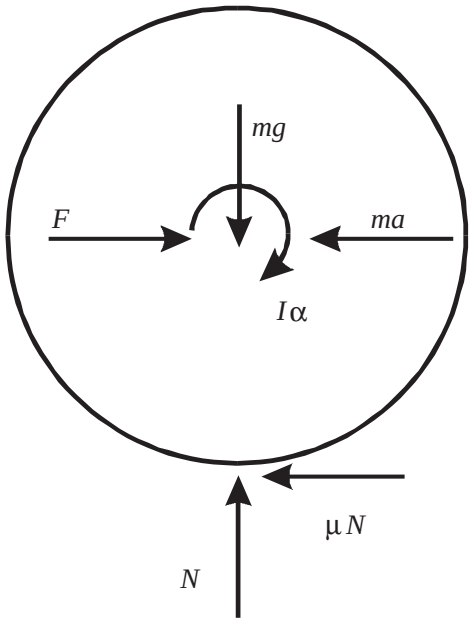

Fig. 11. Dynamic forces on the wheel set.

where R is the radius of the wheel, and $I = I_{yy}$ is the mass moment of inertia of the wheel set. Therefore, if the initial angular velocity of the wheel set is assumed zero, the wheel set angular velocity during the period of sliding is given by the linear expression

$$\omega = \frac{\mu m g R}{I} t. \tag{19}$$

This equation is valid until the wheel set deviates from gross sliding. At the instant of pure rolling, the angular velocity is given by

$$\omega = \frac{V}{R} = 21.88 \text{ rad/s}, \tag{20}$$

where V is the constrained forward velocity of the wheel set. Using Eqs. (19) and (20), the time at which pure rolling starts is given by

$$t_{pr} = \frac{VI}{\mu m g R^2} = 1.05 \text{ s}. \tag{21}$$

A horizontal balance of the forces shown in Fig. 11 yields

$$F = ma + \mu m g. \tag{22}$$

Due to the constant forward velocity constraint, the acceleration of the wheel set and the inertia force are zero. Therefore, the force required to maintain the constant forward velocity during the period of gross sliding is $F = \mu m g = 7.69$ kN. This force is obtained as the Lagrange multiplier associated with the forward velocity driving constraint.

Fig. 12 shows the longitudinal contact force at the left wheel for the hybrid and elastic methods evaluated using Kalker's USETAB routine. The longitudinal contact force shows oscillations when the elastic method is used. For both models, during the period of sliding, the mean value of this force agrees well with the theoretical value ($0.5\,\mu m g = 3.85$ kN). Fig. 13 shows the force associated with the forward velocity driving constraint (Lagrange multiplier). It is clear from the results presented in this figure that during the period of sliding the mean value coincides with the value given previously using the simple analytical analysis.

Fig. 14 shows the lateral displacement of the wheel set. The results show a good agreement between the elastic method and the hybrid method. As shown in the figure, the amplitude of the oscillations increases more rapidly in the results of the hybrid method than in the results of the elastic method. Fig. 15 shows the yaw angle of the wheel set for both models. Klingel's formula [15] gives a hunting frequency of 0.428 Hz for this problem. The frequencies predicted from the multibody dynamic simulation are 0.423 Hz for both the hybrid method and the elastic method. Therefore, the hunting frequency obtained from the simulations is slightly smaller than Klingel's theoretical value.

Fig. 16 shows the time history of the left wheel parameter s_1^w of the contact point for both models. The results of the elastic method show that this parameter changes in finite increments, this is due to the method of the search for the contact point. As previously explained, the contact point is selected from the nodal points that define the wheel profile. Therefore, the use of large number of nodal points leads to smoother results.

Fig. 17 shows the normal contact force at the right wheel for both models. For the hybrid method the force is smoother and oscillates with a mean value equal to half the weight

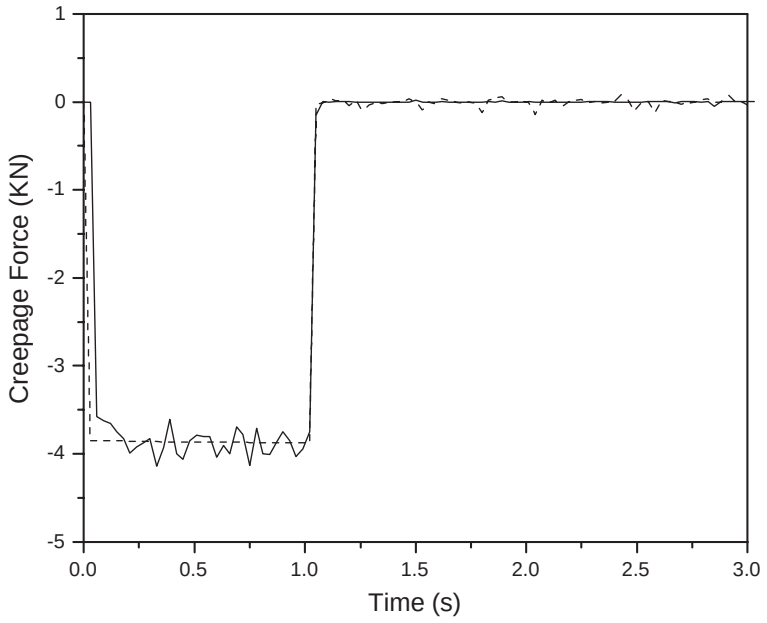

Fig. 12. Longitudinal creepage force acting on the left wheel: —, elastic method; ----, hybrid method.

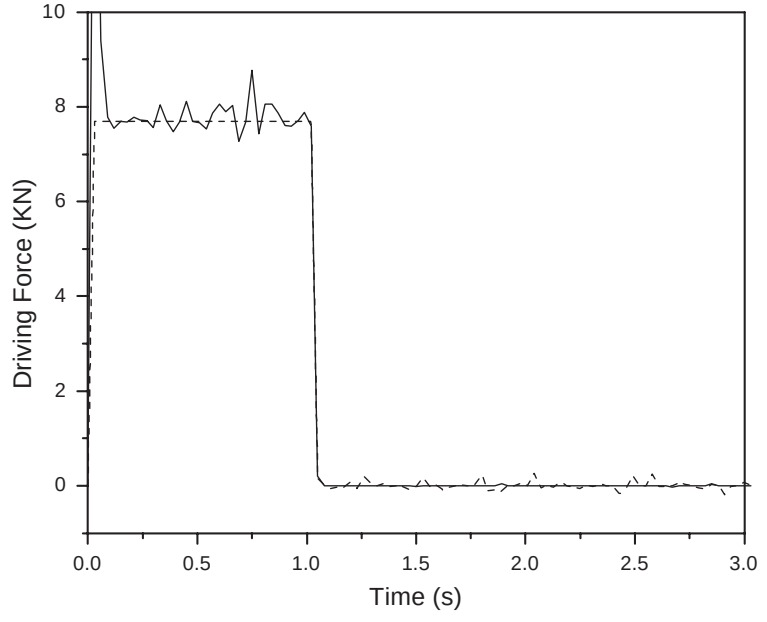

Fig. 13. Driving forward velocity constraint: —, elastic method; ----, hybrid method.

of the wheel set. The frequency of oscillation of the force is the same as the hunting frequency. This effect is due to the lateral displacement, as the wheel set moves laterally to one side the normal contact force increases in that side and decreases in the opposite side [8]. The

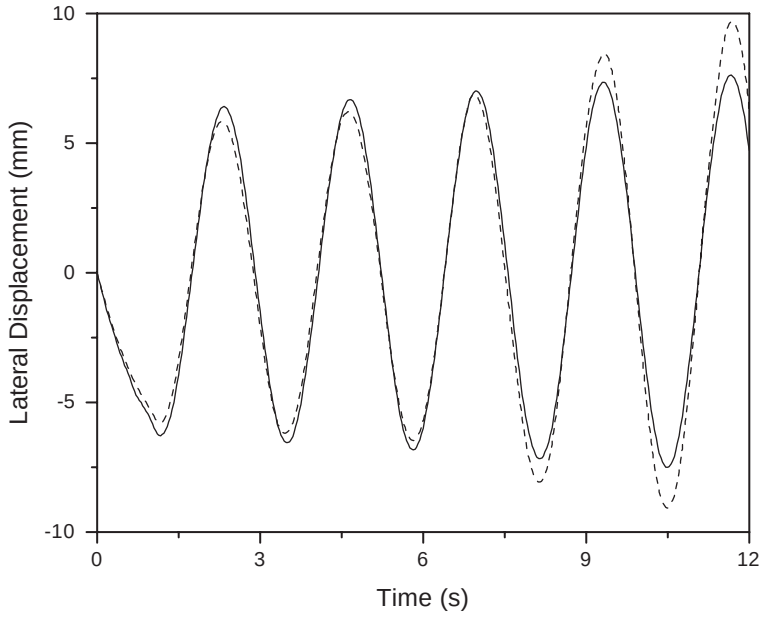

Fig. 14. Lateral displacement of the wheel set: —, elastic method; ----, hybrid method.

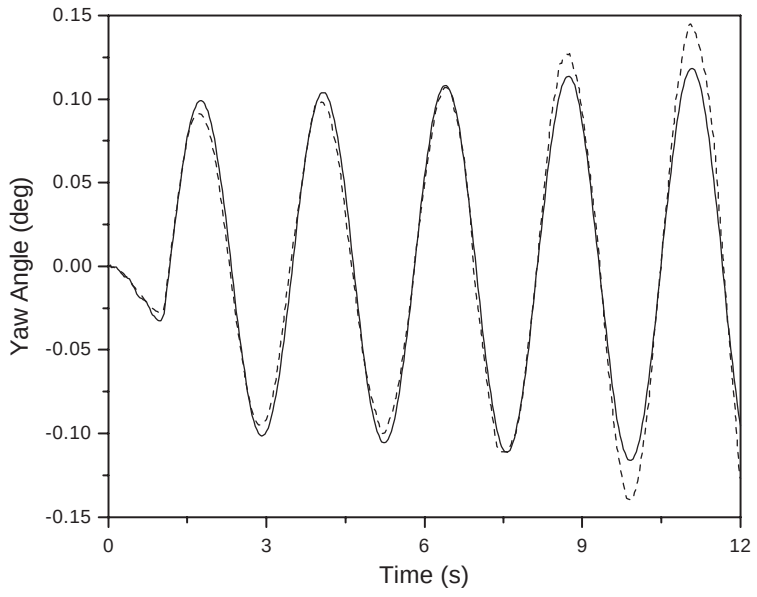

Fig. 15. Yaw angle of the wheel set: —, elastic method; ----, hybrid method.

normal contact force for the elastic method shows high-frequency oscillations superimposed on the low hunting frequency oscillations. The mean value, however, remains half the weight of the wheel set.

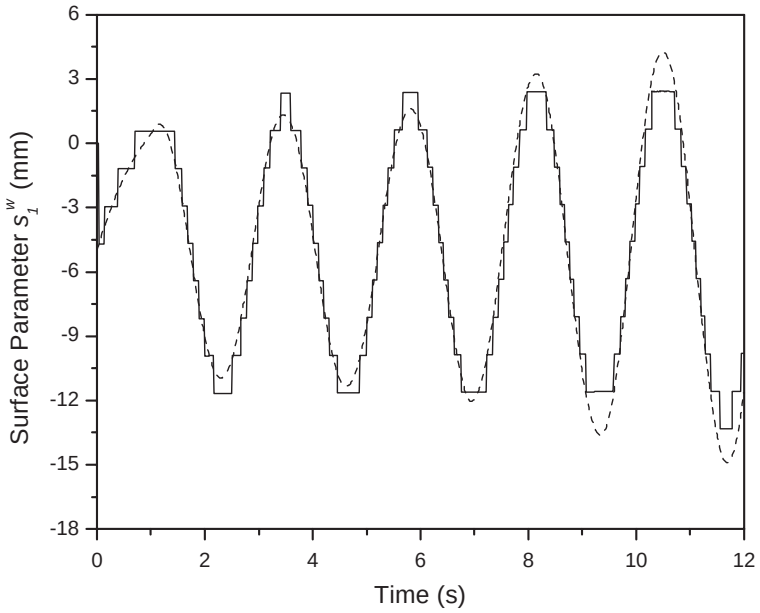

Fig. 16. Wheel parameter s_1^w: —, elastic method; ----, hybrid method.

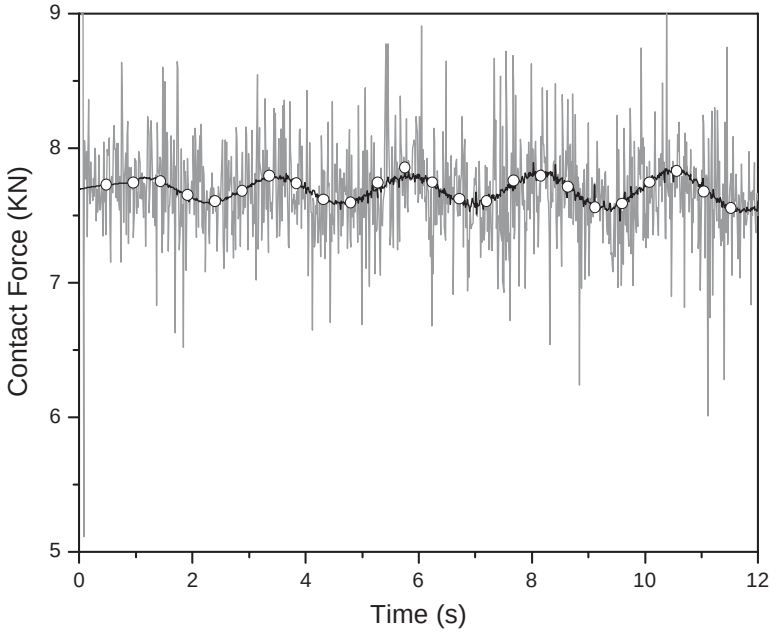

Fig. 17. Normal contact force on the right wheel: ——, elastic method; —○—, hybrid method.

9.2. High-velocity hunting

In this section, the dynamics of the same wheel set is examined when the forward velocity V is increased to 30 m/s. The results are obtained using the two methods: the elastic force model and the hybrid model. In this case, the wheel set is assumed to have an initial rolling angular velocity $\omega_y = 65.6$ rad/s and an initial lateral velocity $v_y = -0.18$ m/s. All other initial conditions are equal to zero. Because of the initial angular velocity the motion starts with pure rolling. Fig. 18 shows the lateral displacement for both models, while Fig. 19 shows the yaw angle. These two figures show a good agreement between the results obtained using the two methods. Klingel's formula gives a hunting frequency of 1.285 Hz for this problem. Using the results of the simulations, the calculated frequencies are 1.484 Hz for the hybrid model and 1.373 Hz for the elastic model. Figs. 18 and 19 show that flange contacts restrict the value of the lateral displacement and yaw angle within certain maximum limits, ± 10 mm and $\pm 0.18^\circ$, respectively. Figs. 20 and 21 show the lateral impact forces at the wheel flanges for both models. It is clear from the results presented in the figures that these forces act at the right and left wheels. Figs. 22 and 23 show the normal contact forces for both models at the tread of the left wheel. As in the previous example, the normal contact forces oscillate with the hunting frequency [8]. Fig. 22 shows that, for the hybrid method, the normal contact force has a jump as the result of the flange impacts. At these instants, the normal contact force has negative (tensile) values (maximum tensile contact forces are not shown in Fig. 22). Clearly, these forces are not physically meaningful, and they are due to the limitation of the constraint model, which does not allow separation between the wheel and the

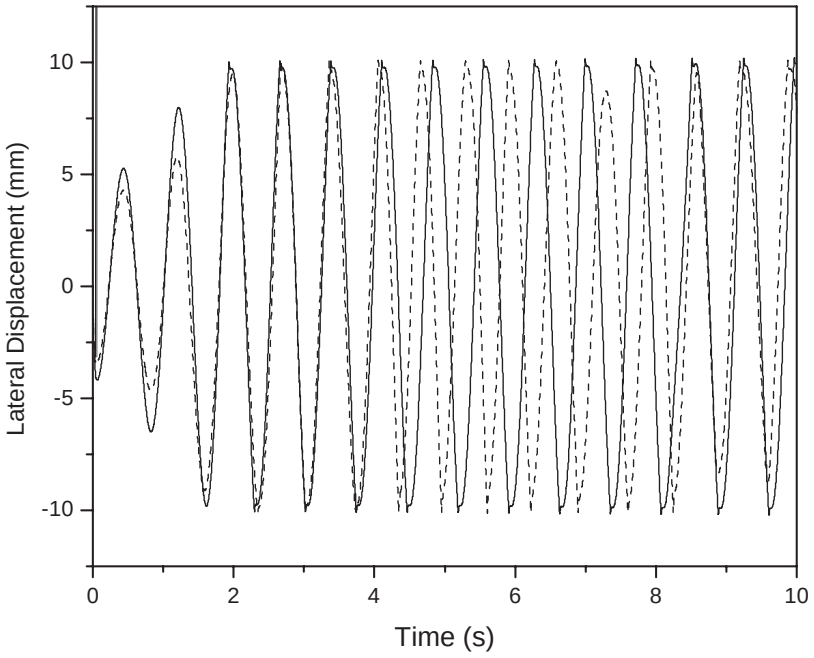

Fig. 18. Lateral displacement: —, elastic method; ----, hybrid method.

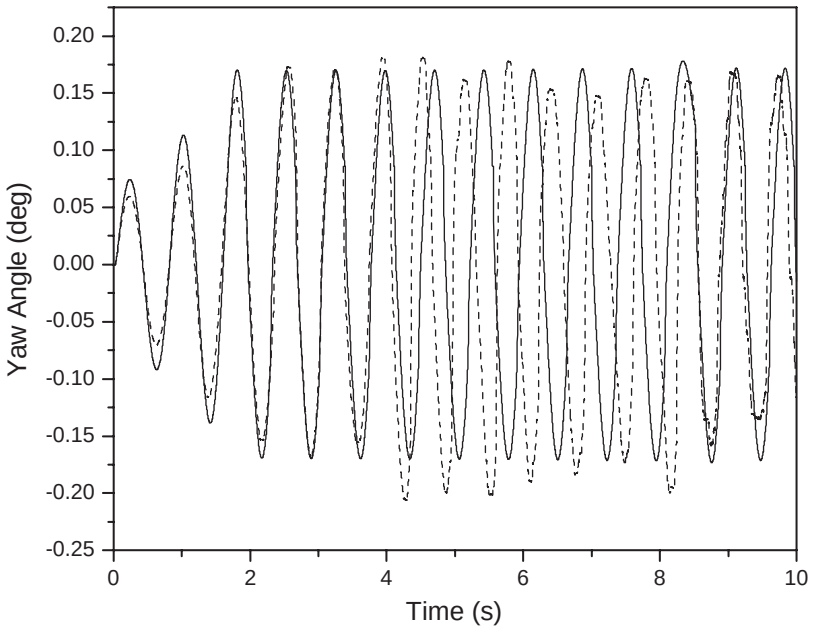

Fig. 19. Yaw angle: —, elastic method; ----, hybrid method.

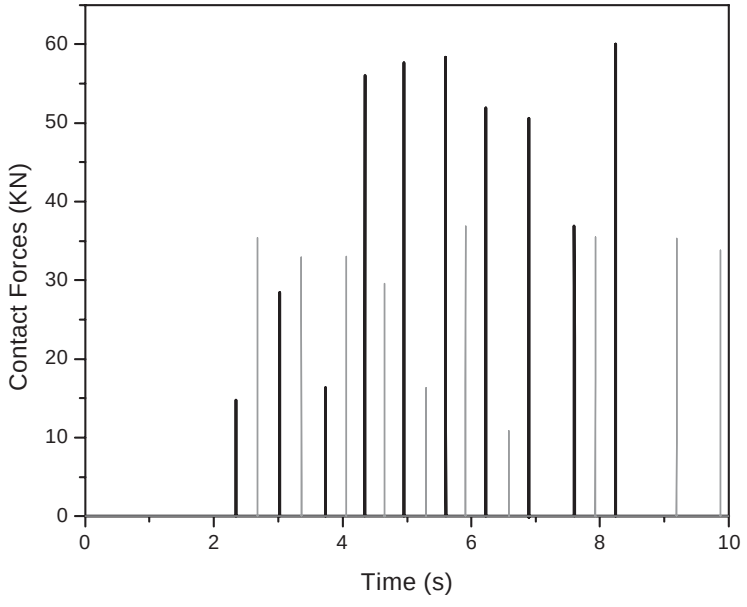

Fig. 20. Flange impact forces (hybrid method): ━━, right wheel; ——, left wheel.

rail. However, such results can be used in the future to develop criteria for wheel/rail separation. The normal contact force given in Fig. 23 for the elastic model shows high-frequency oscillations superimposed on low hunting frequency oscillations. Contact force jumps due to flange impacts

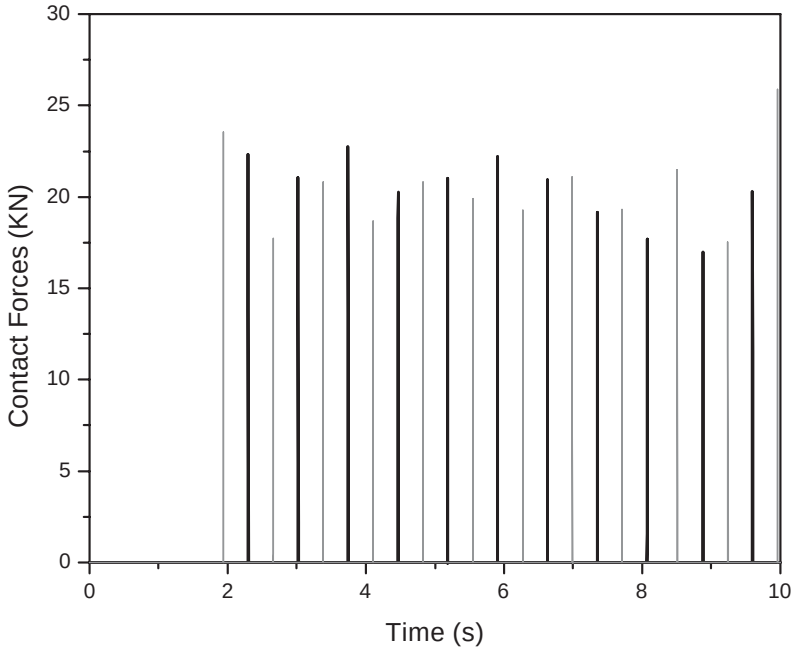

Fig. 21. Flange impact forces (elastic method): ——, right wheel; ——, left wheel.

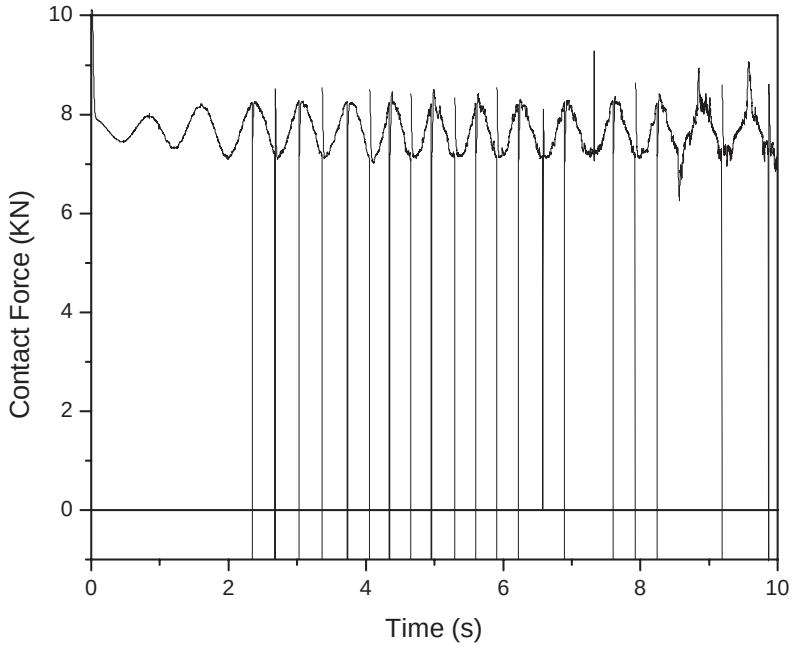

Fig. 22. Normal contact force at left wheel (hybrid model).

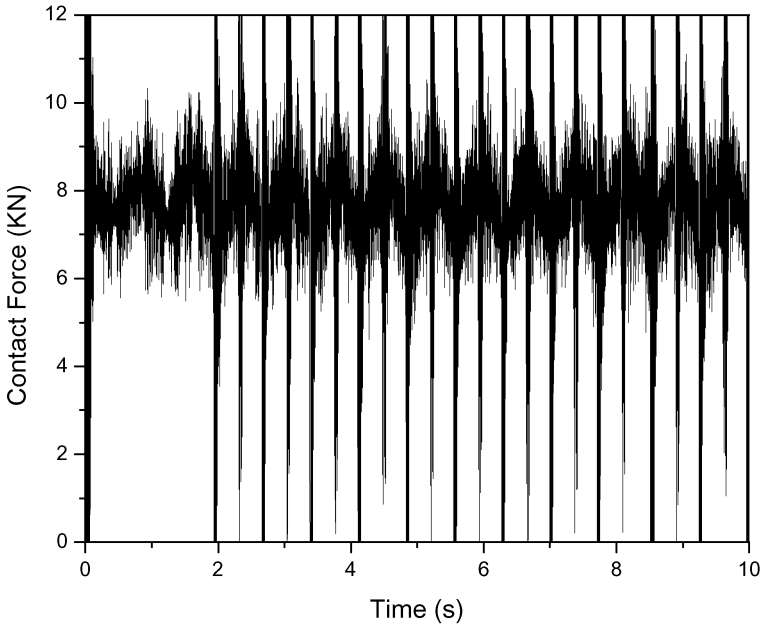

Fig. 23. Normal contact force at left wheel (elastic model).

can also be observed in this figure. However, since the elastic model allows separation, tensile contact forces do no appear.

9.3. Two-point contact in curved track simulation

In this example, the wheel set travels with constant forward velocity $V = 10\,\text{m/s}$ on a curved track. The wheel set and the rail have the same properties used in the previous examples. No constraint is imposed on the yaw rotation of the wheel set. The track has a constant curvature of 5° ($100'$-chord definition) and zero superelevation. Therefore, the radius of curvature R_C is constant and is equal to 350 m. The wheel set is assumed to have an initial rolling angular velocity of $\omega_y = 21.88\,\text{rad/s}$. All other initial conditions are assumed to be equal to zero. As in the previous examples, the results are obtained using the elastic and the hybrid methods.

During a simulation time of 8 s, the wheel set travels 80 m. At that point, the angle between the tangent to the rails and the X global axis is 13°. Fig. 24 shows the motion trajectory of the wheel set. Fig. 25 shows the angle rotated versus time. As shown in Fig. 25, the wheel set rotates about the Z-axis with approximately constant angular velocity. The results obtained using the elastic and the hybrid methods were found to be approximately identical. A short time after the beginning of the simulation, the right wheel encounters two-point contact and maintains this contact with the right rail during the entire simulation, as the result of the centrifugal force. As a consequence, the transverse position of the wheel set with respect to the rail does not change, and, the wheel surface parameters s_1^w and the rail surface parameters s_2^r remain constant. Their values

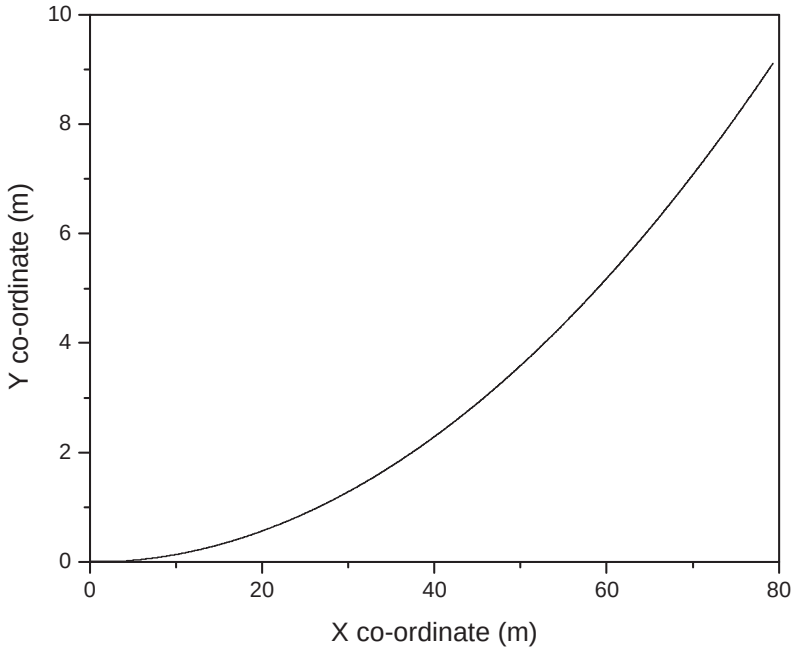

Fig. 24. Wheel set trajectory.

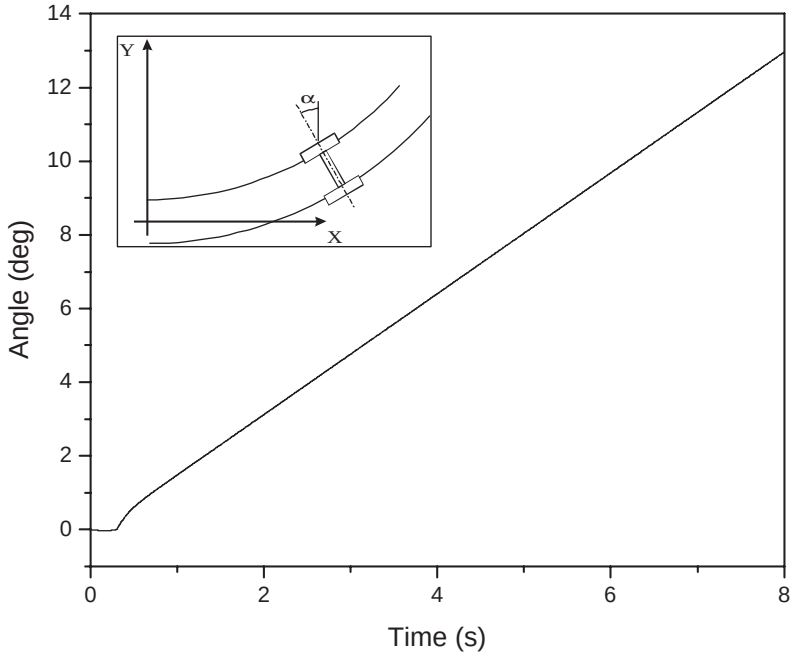

Fig. 25. Angle of rotation.

are given in Tables 1 and 2. The yaw and roll angles of the wheel set also remain approximately constant, their values are given in Table 3 for the hybrid and elastic methods.

Figs. 26 and 27 show the magnitude of the contact forces at the left wheel, including normal and creepage forces, for the elastic and hybrid method, respectively. It is clear that in both models these forces show high-frequency osillations, keeping a constant average value of 8 kN. Figs. 28 and 29 show these forces at the two points of contact at the right wheel. These forces have approximately constant average values of 7 kN for the first contact and 6 kN for the second contact. A good agreement is found between the results of the hybrid and the elastic models. Since the yaw rotation of the wheel set is negative, the second point of contact appears in the leading side of the right wheel. The values of Δs_1^r and Δs_2^w are provided in Table 3 for the hybrid and elastic methods.

Figs. 30 and 31 show a free body diagram of the wheel set with approximate average values of the contact forces in the transverse and longitudinal directions, respectively. The weight and centrifugal forces (mV^2/R_C) are included in Fig. 30. In the vertical direction, the weight of the

Table 1
Surface parameters for the three contacts (elastic method)

Variable	Contact		
	Right wheel (first contact)	Right wheel (second contact)	Left wheel
Rail parameter s_2^r (mm)	2.36	36.95	−2.36
Wheel parameter s_1^w (mm)	7.62	41.55	11.63

Table 2
Surface parameters for the three contacts (hybrid method)

Variable	Contact		
	Right wheel (first contact)	Right wheel (second contact)	Left wheel
Rail parameter s_2^r (mm)	3.29	36.95	−3.16
Wheel parameter s_1^w (mm)	8.00	41.55	11.50

Table 3
Relative position of the wheel set

Variable	Method	
	Elastic method	Hybrid method
Yaw angle (deg)	−0.1031	−0.0974
Roll angle (deg)	−0.0188	−0.0206
Δs_1^r (mm)	4.10	3.73
Δs_2^w (deg)	0.499	0.454

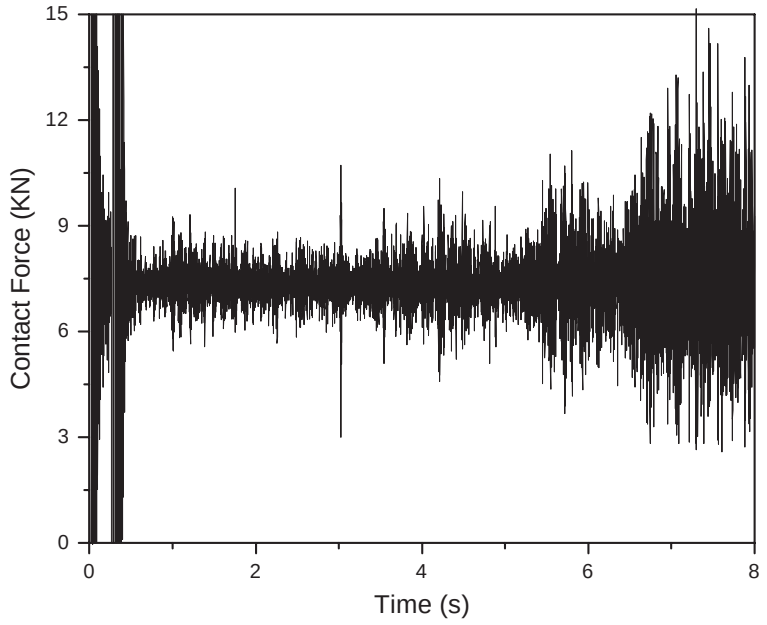

Fig. 26. Contact force on the left wheel (elastic model).

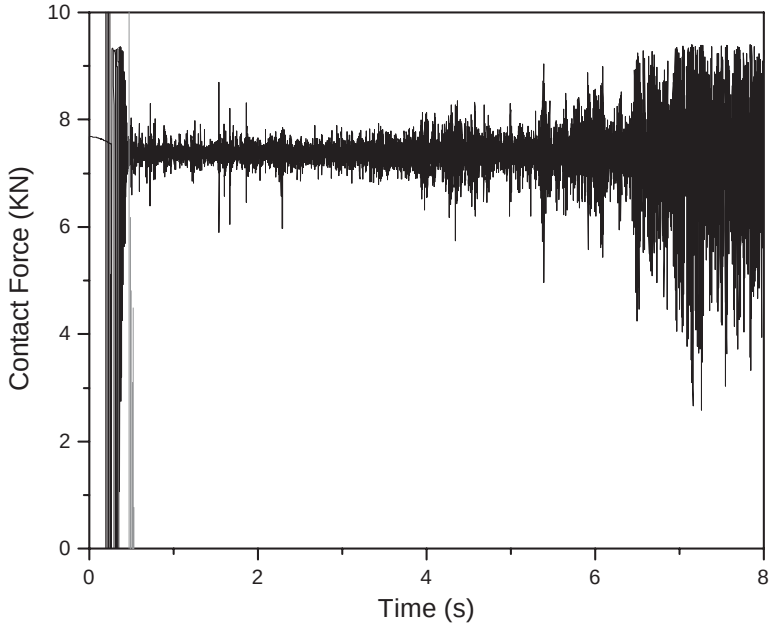

Fig. 27. Contact force on left wheel (hybrid model).

wheel set is balanced by vertical forces at the three contacts (F_Z^L, F_Z^R and F_Z^F), with the larger values occurring at the first contacts. The force balance in the horizontal direction shows an interesting result. It can be seen that the horizontal contact force on the flange of the right wheel

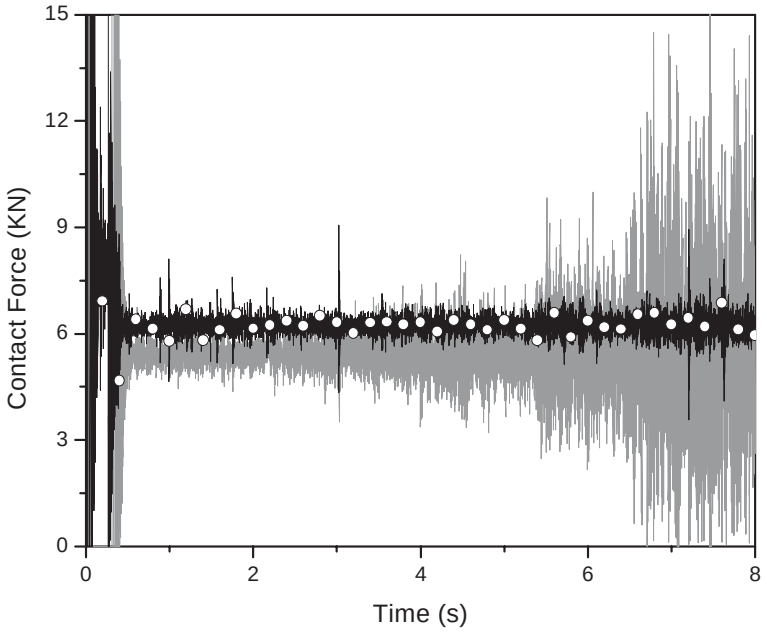

Fig. 28. Contact forces on right wheel (elastic model): —○—, first contact; ——, second (flange) contact.

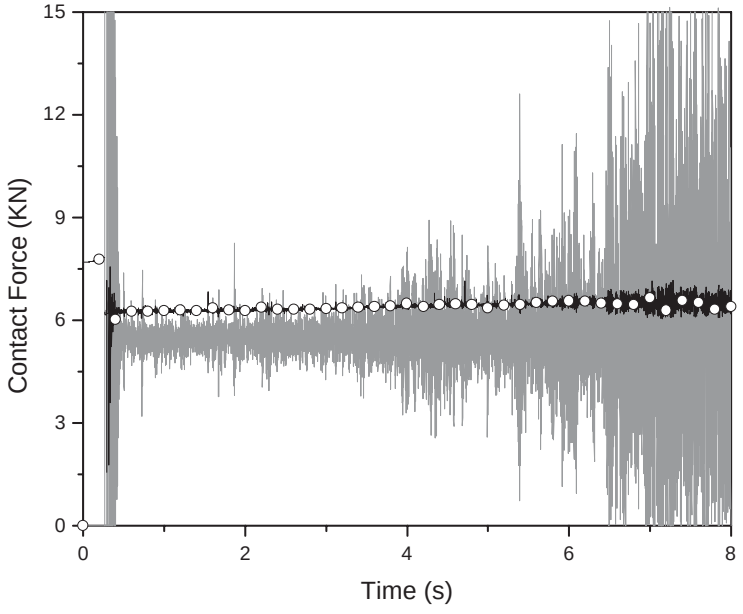

Fig. 29. Contact forces on right wheel (hybrid model): —○—, first contact; ——, second (flange) contact.

(F_Y^F) is more than 10 times the centrifugal force. This is due to the occurrence of very large friction forces at the main contacts (F_Y^L,F_Y^R). As a consequence, a very large dynamic friction force (F_X^F) is generated at the flange of the right wheel in the longitudinal direction (see Fig. 31). This dynamic

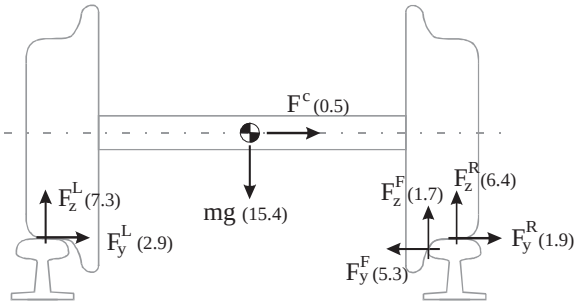

Fig. 30. Free body diagram of the wheel set (transverse direction).

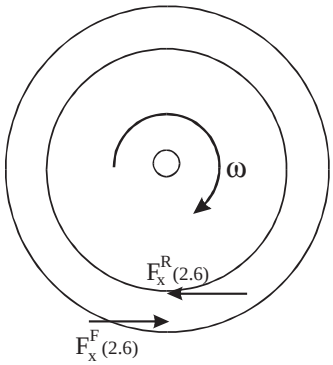

Fig. 31. Free body diagram of the wheel set (longitudinal direction).

friction force has the value given by the Coulomb friction theory, $F_X^F = \mu F^F$, with $\mu = 0.5$ is the assumed coefficient of friction. This friction force at the flange is balanced by a friction force F_X^R at the first contact between the rail and the wheel. Simulation results show that the longitudinal contact force at the left wheel and the force due to the forward velocity constraint (both forces should be included in Fig. 31) are very small (less than 0.1 kN). The previous force balance, based on the simulation results, shows that the energy lost due to dynamic friction at the flange of the wheel can be much larger (almost ten times) than that obtained with the assumption that the flange horizontal force is equal to the centrifugal force.

10. Summary and conclusions

In this paper, a new elastic force contact formulation for the dynamic simulation of the wheel/rail interaction is presented. In this contact formulation, four surface parameters are introduced in order to be able to describe the geometry of the surfaces of the two bodies that come in contact. The method developed in this investigation exploits features of multibody computational algorithms that allow adding arbitrary first order differential equations. A differential equation associated with the rail arc length and expressed in terms of the wheel generalized co-ordinates

and velocity is used to accurately predict the location of the points of contact between the wheel and the rail. This first order differential equation is integrated simultaneously with the dynamic equations of motion of the wheel/rail system, thereby defining the rail arc length travelled by the wheel. This arc length is used with an optimized search algorithm to determine all possible contact regions. By determining the local co-ordinates of the contact points and knowing the arc length surface parameter, the other surface parameters can be determined and used to determine the principal curvatures of the wheel and the rail at the contact points. These principal curvatures with the penetration and the material properties of the wheel and the rail are used to determine the normal contact forces. The non-linear creepages and the normal contact forces are used to determine the creep forces that in turn are used to determine the generalized creep forces associated with the system generalized co-ordinates.

The elastic force approach proposed in this study differs from the contact constraint approach [7,8] in which five non-linear algebraic constraint equations are used to impose the contact conditions. These equations are expressed in terms of the generalized co-ordinates and non-generalized surface parameters. The contact constraint equations are augmented to the differential equations of motion using the technique of Lagrange multipliers. The augmented form of the equations of motion can be solved for the second derivatives of the generalized co-ordinates and non-generalized surface parameters as well as Lagrange multipliers. Lagrange multipliers associated with the contact constraints are used to predict the normal contact forces. As discussed in this paper and in previous investigations [7,8], the use of the general contact constraint formulation requires the evaluation of third derivatives with respect to the surface parameters. As a result, smoothness and differentiability of the constraint equations become an important issue when this procedure is used.

The results obtained using the elastic force formulation proposed in this investigation and the contact constraint formulation are compared using a wheel set travelling on tangent and curved tracks. Two methods are proposed to study the two-point contact problem; the elastic method and the hybrid method. Results presented in this paper show, in general, good agreement between the results of the two methods. In general, the contact forces obtained using the elastic method have high-frequency oscillations that are not present in the constraint method.

Acknowledgements

This research was supported by the Federal Railroad Administration, Washington, D.C. and in part by the Fulbright Foundation; and the Spanish Ministry of Education, Culture and Sports.

References

[1] J.J. Kalker, Survey of wheel–rail rolling contact theory, Vehicle System Dynamics 8 (4) (1979) 317–358.
[2] J.C. Samin, L. Neuve, A multibody approach for dynamic investigation of rolling systems, Ingenieur-Archiv 54 (1984) 1–15.
[3] A.D. De Pater, The geometrical contact between track and wheel-set, Vehicle System Dynamics 17 (1988) 127–140.
[4] B. Simeon, C. Fuhrer, P. Rentrop, Differential-algebraic equations in vehicle system dynamics, Survey on Mathematics in Industry 1 (1991) 1–37.

[5] W. Kortum, R.S. Sharp, Multibody computer codes in vehicle system dynamics, Supplement to Vehicle System Dynamics 22 (1993) 1–276.
[6] K. Popp, W. Schiehlen, Fahrzeugdynamik, B.G. Teubner, Stuttgart, 1993.
[7] A.A. Shabana, J.R. Sany, An augmented formulation for mechanical systems with non-generalized co-ordinates: application to rigid body contact problems, Journal of Nonlinear Dynamics 24 (2001) 183–204.
[8] A.A. Shabana, M. Berzeri, J.R. Sany, Numerical procedure for the simulation of wheel/rail contact dynamics, American Society of Mechanical Engineers, Journal of Dynamic Systems, Measurement, and Control 123 (2001) 168–178.
[9] W. Kik, J. Piotrowski, A fast, approximate method to calculate normal load at contact between wheel and rail and creep forces during rolling, in: I. Zabory (Ed.), Proceedings of the Second Mini Conference on Contact Mechanics and Wear of Rail/Wheel System, Budapest, 1996.
[10] W. Kik, H. Steinborn, Wheel/rail connexion-element for use in a multi-body-algorithm, Dynamics of Vehicles on Roads and Tracks, Proceedings of the Eighth IAVSD Symposium, Cambridge, MA, USA, 1984, pp. 303–316.
[11] A.A. Shabana, Computational Dynamics, 2nd Edition, Wiley, New York, 2001.
[12] M. Berzeri, R.J. Sany, A.A. Shabana, Curved track modeling using the absolute nodal co-ordinate formulation, Technical Report No. MBS00-4-UIC, University of Illinois at Chicago, 2000.
[13] K.L. Johnson, Contact Mechanics, Cambridge University Press, Cambridge, 1985.
[14] T.W. Lee, A.C. Wang, On the dynamics of intermittent motion mechanisms, Part I. Dynamic model and response, Journal of Mechanisms, Transmissions and Automation in Design 105 (1983) 534–540.
[15] W. Klingel, Über den Lauf von Eisenbahnwagen auf gerarder Bahn, Organ für die Fortschritte des Eisenbahnwesens 20 (1883) 113–123.